ELSEVIER

Effect of temperature uncertainty on polymer electrolyte fuel cell performance ☆

CrossMark

Mozhdeh Noorkami [a], James B. Robinson [a], Quentin Meyer [a],
Oluwamayowa A. Obeisun [a], Eric S. Fraga [a], Tobias Reisch [b],
Paul R. Shearing [a], Daniel J.L. Brett [a,*]

[a] Electrochemical Innovation Lab, Department of Chemical Engineering, UCL, Torrington Place, London WC1E 7JE, United Kingdom
[b] Intelligent Energy, Charnwood Building, Holywell Park, Ashby Road, Loughborough, Leicestershire LE11 3GB, United Kingdom

ARTICLE INFO

ABSTRACT

The temperature of operation is a key parameter in determining the performance and durability of a polymer electrolyte fuel cell (PEFC). Controlling temperature and understanding its distribution and dynamic response is vital for effective operation and design of better systems. The sensitivity to temperature means that uncertainty in this parameter leads to variable response and can mask other factors affecting performance. It is important to be able to determine the impact of temperature uncertainly and quantify how much PEFC operation is influenced under different operating conditions. Here, a simple lumped mathematical model is used to describe PEFC performance under temperature uncertainty. An analytical approach gives a measure of the sensitivity of performance to temperature at different nominal operating temperatures and electrical loadings. Whereas a statistical approach, using Monte Carlo stochastic sampling, provides a 'probability map' of PEFC polarisation behaviour. As such, a polarisation 'area' or 'band' is considered as opposed to a polarisation 'curve'. Results show that temperature variation has the greatest effect at higher currents and lower nominal operating temperatures. Thermal imaging of a commercial air-cooled stack is included to illustrate the temporal and spatial temperature variation experienced in real systems.

Copyright © 2013, The Authors. Published by Elsevier Ltd. All rights reserved.

1. Introduction

A polymer electrolyte fuel cell (PEFC) is a device that converts chemical energy in fuels directly into electricity with high efficiency, no combustion or moving parts [1]. The advantages of this type of fuel cell includes low operating temperature, quick start-up, planar configuration and easier sealing due to the use of a solid electrolyte [2—9]. However, water management issues require careful consideration to ensure good protonic conductivity in the electrolyte while avoiding electrode flooding that limits reactant access and results in mass

* Corresponding author. Tel.: +44 (0) 20 7679 3310.
E-mail address: d.brett@ucl.ac.uk (D.J.L. Brett).
URL: http://www.ucl.ac.uk/electrochemical-innovation-lab

transport limitations [10]. To achieve this, it is important to run the system at the optimum operating conditions by applying efficient control methodologies. There are many factors which affect performance, ranging from fundamental thermodynamic properties; ionic, electronic and mass transport mechanisms; heat transfer and electro-kinetics [11–13]. For all these processes, temperature is a major determining factor and control is essential for understanding how fuel cells operate, optimising performance, and developing better and longer lasting devices.

When operating fuel cells, there is always a level of 'uncertainty' in the operating parameters and physical state of the system that leads to variable and unpredictable performance. This uncertainty can be due to fluctuations and distribution of operating parameters, measurement accuracy, random errors, unoptimised/unstable control, etc. [14]. Temperature is one of the parameters with the highest uncertainty as it is a function of operating point, reactant flow rate and ambient conditions; it is also temporally variant under dynamic conditions and spatially heterogeneous.

The sensitivity of fuel cell operation with respect to temperature has been reported in the literature [15–17]. Studies have focussed on the impact of operating temperature on fuel cell performance, and also uncertainty as a part of the control system [18,19].

Temperature is an important component in fuel cell operation, and plays a key role in cell performance [20,21]. Water transport is directly influenced by temperature, affecting the mobility of species in the electrolyte and access and removal of water at the electrodes and propensity to flooding [10]. Thermal imaging has increasingly become a popular tool for the investigation of fuel cells. It provides high spatial resolution imaging and allowing non-contact measurements, so avoiding potential interference with fuel cell operation. Thermal imaging can be used to identify defects and/or areas of unusually low or high activity on the surface of fuel cells. Aieta et al. have shown how catalyst loading defects can be investigated using thermal imaging [22]. Hakenjos et al. measured the current and temperature distribution using IR thermography in order to obtain the temperature distribution along the GDL of a PEMFC [23]. They also observed flow-field flooding through images taken from temperature distribution. Daino et al. have performed similar work aimed at identifying temperature gradients along GDL layers within PEMFCs [24].

In this paper, a simple mathematical lumped model is used to examine the effect of temperature on the parameters and fundamental physical and chemical properties that determine PEFC performance. First, an analytical approach is adopted that examines the sensitivity of the equations to small changes in temperature by using the differential dV/dT to map the operating range of polarisation and nominal operating temperature. However, this does not capture the stochastic nature of the uncertainty associated with practical operation, so a second analysis is performed that applies a statistical treatment to develop a 'probability map' of fuel cell polarisation performance.

In order to support the statistical study, an experimental characterisation of a commercial air-cooled stack is performed that uses high-resolution thermal imaging to characterise the kind of spatial and temporal temperature uncertainty that can be expected in a practical operating system.

The intention of this study is to provide fuel cell developers with a basis for estimating the expected level of uncertainty in polarisation performance based on a given uncertainty in the temperature of the system (spatial and temporal). A key outcome is that conventional polarisation curves should be considered as 'polarisation areas' or 'bands' with variable uncertainty across their operating range.

1.1. Temperature uncertainty in fuel cell operation

Temperature distribution within fuel cells has been modelled using a range of techniques and length scales; for example, Shimpalee and Dutta describe the temperature variation across the flow channel width [21] and Pharoah and Burheim at the cell level [20]. However, models rarely consider the effect of measurement and physical uncertainty on cell performance.

Mawardi and Pitchumani investigated the impacts of uncertainty in materials and operating parameters on fuel cell performance by using a one dimensional, non-isothermal mathematical model [14]. Parametric analysis was used to determine how cell voltage and power density change with uncertainty, where the input samples were generated stochastically using the Latin Hypercube Sampling (LHS) method.

To show the significance of temperature on other variables like degradation rate, Placca et al. demonstrated the effect of the interaction between temperature and degradation rate on overall performance of fuel cells [25]. The Response Surface Method (RSM) was applied in this study to analyse the effect of uncertainty in these variables on polarisation (V–I) curves. However, no attempt was made to quantify the association between the measurement uncertainty and temporal and spatial temperature distribution.

2. Model development

For the purpose of analytical and statistical analysis, a mathematical model is required to describe the thermodynamics of the system, kinetics, mass and charge transfer as a function of temperature.

2.1. Model assumptions and equations

A lumped, semi-empirical, mathematical model is used to simulate PEFC operation [10,11]. The purpose of using this model is to indicate the effect of temperature on different parameters and identify their impact on overall performance. Therefore, some of the parameters, such as exchange current density and conductivity, which are usually measured experimentally, are expressed using empirical equations, which themselves can generate discrepancy due to model uncertainty. However, the focus of this work is the impact of temperature uncertainty on cell performance, whereas model uncertainty is assumed negligible. The following assumptions are applied: (i) steady state system; (ii) incompressible and ideal gases; (iii) single phase vapour water; (iv) heat loss is

negligible; (v) pressure drop is negligible; (vi) current distribution is uniform; and (vii) there is no reactant consumption along the length of the flow channel (reactant distribution is homogeneous).

Simple lumped models of PEFC operation are well documented and have been used for a wide variety of applications [11]. The model used here follows a well-established protocol with the key equations summarised in Table 1 [10,26–29], and the physical constants and parameters defined in Table 2 [10,11,17,25–28]. The important role of temperature in determining PEFC performance is evident by the common appearance of T in the governing equations, which include logarithmic, exponential, power and linear functions.

As is commonly used in fuel cell modelling, the empirical Bruggeman correlation was used to estimate conductivity and diffusivity [30–32]. However, this assumes that there is no liquid water present in the cell. At low temperature and high current density there is a higher chance of liquid water

Table 2 – Physical constants used in the model.

Parameter	Value
Catalyst loading (L_c)	0.125 mg(Pt) cm^{-2}
Catalyst-specific area (a_{ca})	0.4 cm^2 mg^{-1}
Faraday's constant (F)	96,486 C mol^{-1}
Ideal gas constant (R)	8.314 J mol^{-1} K^{-1}
Membrane thickness (l)	0.01275 cm
Reference exchange current density (i_0^{ref})	3×10^{-9} A cm^{-2}
Reference temperature (T_{ref})	298 K
Reference pressure (P_{ref})	1 atm
Reference Gibbs free energy (G_{ref})	$-228,170$ J mol^{-1}
Activation energy (E_c)	76,500 J mol^{-1}
Diffusion coefficient of water in membrane (D_0)	5.5×10^{-7} cm^2 s^{-1}
Active area (A)	25×10^4 cm^2
Operating pressure (P)	1.5 atm
Oxygen pressure (P_{O_2})	5 atm
Hydrogen pressure (P_{H_2})	3 atm
Water pressure (P_w)	1 atm
Reference binary diffusion coefficient (D_{ij}^{ref})	0.1 cm^2 s^{-1}
GDL thickness (t_{GDL})	0.05 cm
Enthalpy change (dH)	$-242,367.25$ J
Entropy change (dS)	-84.2 J
Cathode water activity (α_c)	0.3
Anode water activity (α_a)	0.5
Porosity (ε)	0.444
Number of electrons at cathode (n_c)	4
Number of electrons at anode (n_a)	2
Relative humidity of air (RH_{air})	0.5
Relative humidity of fuel (RH_{fuel})	1
Stoichiometric ratio of hydrogen (λ_{H_2})	1.25
Stoichiometric ratio of oxygen (λ_{O_2})	2
Pressure coefficient (γ)	0.5
Oxygen mole fraction (x_{O_2})	0.21

Table 1 – List of equations used to describe the physical mode of the PEFC.

Name	Equations
Species mass flux	$M_{H_2} = \lambda_{H_2}\frac{iA}{n_aF}$ $M_{O_2} = \lambda_{O_2}\frac{iA}{n_cF}$ $M^v_{H_2O,c} = \left\| \frac{y_{H_2O_{in}}}{1-y_{H_2O_{in}}}\right\|_c M_{O_2}$ $M^v_{H_2O,a} = \left\| \frac{y_{H_2O_{in}}}{1-y_{H_2O_{in}}}\right\|_a M_{H_2}$ $y_{H_2O,a} = RH_{fuel}\frac{P^{sat}_{H_2O}}{P}$ $y_{H_2O,c} = RH_{air}\frac{P^{sat}_{H_2O}}{P}$
Thermodynamic	$E_0 = \frac{dH-TdS}{nF}$ $E_{rev} = E_0 - \frac{RT}{nF}\ln\left(\frac{P_{H_2O}}{P_{H_2}P^{0.5}_{O_2}}\right)$ $P^{sat}_{H_2O} = \exp((2.95\times10^{-2})T - (9.18\times10^{-5})T^2$ $+(1.44\times10^{-7})T^3 - 2.18)$
Activation loss at the electrodes	$i_0 = i_0^{ref}a_cL_c\left(\frac{Pr_{O_2}}{Pref}\right)^\gamma \exp\left(\frac{-E_c}{RT}\left(1-\frac{T}{T^{ref}}\right)\right)$ $Pr_{O_2} = \frac{P_{air}}{\exp\left(\frac{4.192i}{T^{1.344}}\right)} - P_{H_2O}$ $\eta_{act} = \left[\frac{RT}{\alpha nF}\ln\frac{i}{i_0}\right]_a + \left[\frac{RT}{\alpha nF}\ln\frac{i}{i_0}\right]_c$
Ohmic loss at the membrane	$\kappa_{mem} = (0.00514c_m - 0.000326)$ $\exp\left(1268\left(\frac{1}{303}-\frac{1}{T}\right)\right)$ $c_m = 0.043 + 17.18a_m - 39.85a_m^2 + 36a_m^3$ $a_m = \beta a_a + (1-\beta)a_c$ $a_a = \frac{M^v_{H_2O,a}}{M^v_{H_2O,a}+M_{H_2}}\cdot\frac{P}{P^{sat}_{H_2O}}$ $a_c = \frac{M^v_{H_2O,c}}{M^v_{H_2O,c}+M_{O_2}}\cdot\frac{P}{P^{sat}_{H_2O}}$ $\eta_{ohmic} = R\cdot i = \frac{l_{mem}}{\kappa_{mem}}\cdot i$
Concentration loss at the electrodes	$i_{L,c} = n_cFD^{eff}\frac{c_{O_2}}{\delta_{GDL}}$ $D^{eff} = D_{O_2/N_2}\varepsilon^{1.5}$ $D_{O_2/N_2} = D^{ref}_{O_2/N_2}\left(\frac{T}{T^{ref}}\right)^{3/2}\left(\frac{pref}{P}\right)$ $C_{O_2} = x_{O_2}\frac{P}{RT}$ $\eta_{con} = \left[\frac{RT}{\alpha nF}\ln\frac{i_L}{i_L-i}\right]_a + \left[\frac{RT}{\alpha nF}\ln\frac{i_L}{i_L-i}\right]_c$

formation. Under such conditions fuel cell performance may be more sensitive to temperature uncertainty and theoretical correlations such as those described by Das et al. may be considered [33].

The overall polarisation curve is generated by subtracting the relevant over-potentials from the open circuit potential:

$$V = E_{rev} - \eta_{act} - \eta_{ohmic} - \eta_{con} \qquad (1)$$

where, E_{rev} is open circuit voltage at zero current density. The Nernst equation is used to describe the thermodynamics. η_{act} is the activation loss due to kinetics of reaction, which depends on the rate of the reactions at the surface of the electrodes. η_{ohm} is the ohmic loss taken to be exclusively due to the ionic resistance of the electrolyte membrane, which is a function of water content and temperature. η_{con} is concentration loss and is a function of the activity of reactants and products and also rate of diffusion of species through the GDL.

2.2. Analytical treatment

The effect of operating temperature on PEFC performance is commonly reported in the range of 30–80 °C [15–17,34], with Das et al. showing that the effect is most significant at high current densities [34].

To determine the sensitivity of cell voltage, based on the intrinsic physics of the system, with respect to temperature and current density, the differential of cell voltage with

Table 3 – Variance of error as a function of sample and bin size.

Sample size	Bin size	V_{error}
100	10	0.5
1000	100	0.158
10,000	1000	0.05
100,000	10,000	0.0158

respect to temperature is determined by applying a small change in temperature (0.05 °C) to the model equations, such that:

$$\frac{dV}{dT} \approx \frac{V_2 - V_1}{T_2 - T_1} \tag{2}$$

2.3. Statistical treatment

To predict the probabilistic deviation of cell voltage due to uncertainty in temperature, a statistical analysis is used that employs a Monte Carlo Simulation (MCS) to provide a random normal distribution of temperature samples. A normal distribution (Gaussian) is employed to describe the statistical spread (uncertainty) of temperatures [35].

To establish the effect of temperature, the standard deviation of ±5 °C is selected for 10,000 samples. Previous studies have reported 3–11 °C temperature variation in a fuel cell due to different uncertainties and operating conditions [20,21,25]. Also, the tests carried out on the commercial stack suggests that this is an appropriate base-case for examining temperature uncertainty.

It is important to choose a suitable sample size which is large enough to give sufficient confidence in the results, but not so large as to lead to unnecessary processing time. To assess this, the model was run from 100 to 100,000 samples in order to develop a distribution curve.

Table 3 shows how different sample size and bin size can affect the variance of error (V_{error}). A sample size of 10,000 was chosen as a suitable trade-off between accuracy and processing time.

To generate the samples, Equation (3) [36] is implemented in Octave (GNU Octave), a high level programming language that provides access to a number of solvers for linear and nonlinear numerical computations [37].
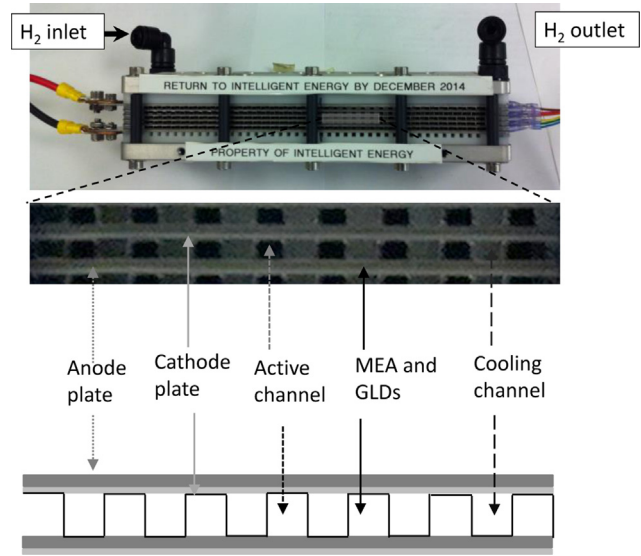
$$T = T_{mean} + \sigma \cdot randn(n, m) \tag{3}$$

Fig. 2 – Picture and sketch of the fuel cell stack showing the active and cooling channels.

where T_{mean} is the mean operating temperature and σ is the standard deviation of distribution.

The obtained data are characterised by statistical analysis: skewness and coefficient of variance (CV), to present the degree of asymmetry of the distributions and measure of dispersion of voltage. Positive skew has a longer tail on the right hand side (higher values) of the mean value and negative skew is bias towards lower values. A distribution curve is classified as symmetrical when the skewness is zero. Because of the nature of the model and logarithmic expressions used in the model, Equation (4) is used to calculate the skewness, where N is the total number of samples [38]:

$$skewness = \frac{\left(\sum (x - \mu(x))^3 \right) / N}{\sigma^3} \tag{4}$$

To verify the skewness, Equation (5) is used to indicate the degree of skewness by comparing the obtained values with the standard error of skew (SES) [39].

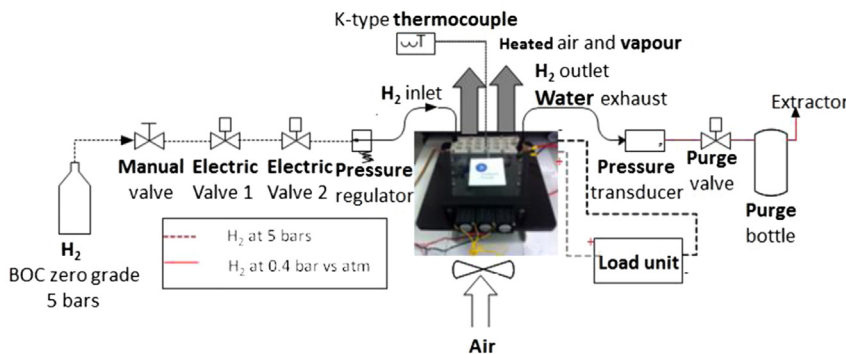$$SES = \sqrt{\frac{6}{N}} \tag{5}$$

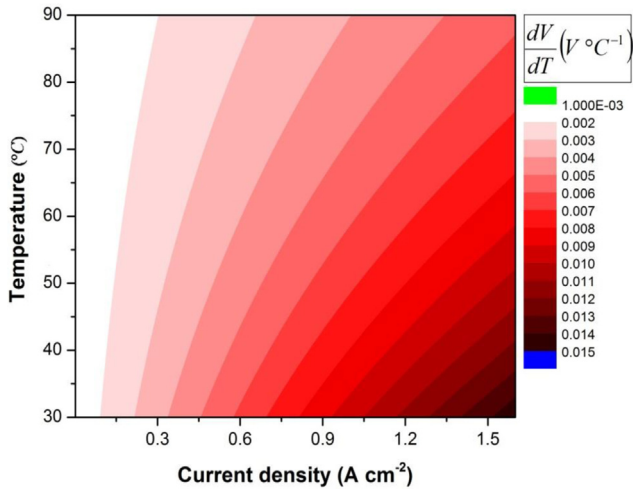**Fig. 1 – Experimental test station for the 5 cell stack.**

Fig. 3 – Sensitivity map based on analytical analysis showing differential change in voltage with temperature (dV/dT) as a function of nominal operating temperature and current density.
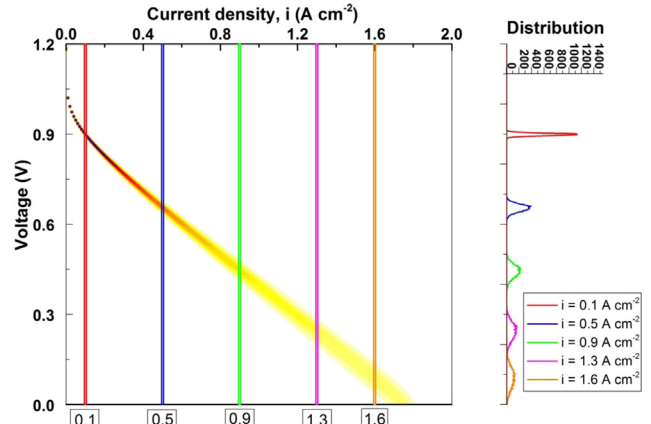

Fig. 5 – Contour plot of V–I polarisation 'area' at mean operating temperature of 80 °C with standard deviation of ±5 °C generated by MCS. Plot to the right hand side shows the voltage distribution at current density of 0.1, 0.5, 0.9, 1.3, and 1.7 A cm^{-2}.

The coefficient of variance (CV), which is often expressed as a percentage, is used to compare the standard deviation of data at diverse mean values [14], where σ is standard deviation of distribution and μ is the mean value [40].

$$CV = \frac{\sigma}{\mu} \tag{6}$$

3. Experimental

3.1. Stack operation

Fuel cell stack operation was carried out using a 5-cell air cooled (AC) open-cathode stack (Intelligent Energy Ltd., UK) [41,42].

This test station, displayed Fig. 1, is used to supply dry, non-heated, pressurized hydrogen in dead-ended mode to the anodes, and oxygen is supplied to the cathode using three fans blowing ambient air through the open cathodes (stack and channel
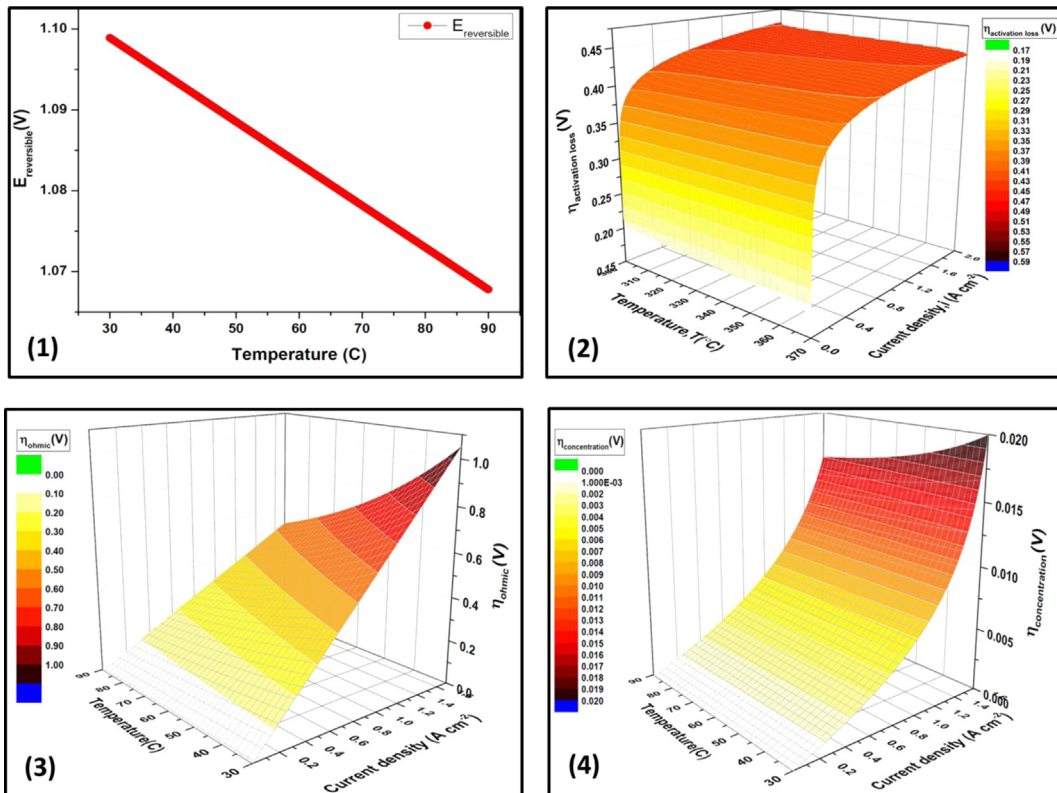

Fig. 4 – Effect of temperature on (1) OCV, (2) activation loss, (3) Ohmic loss and (4) concentration loss.
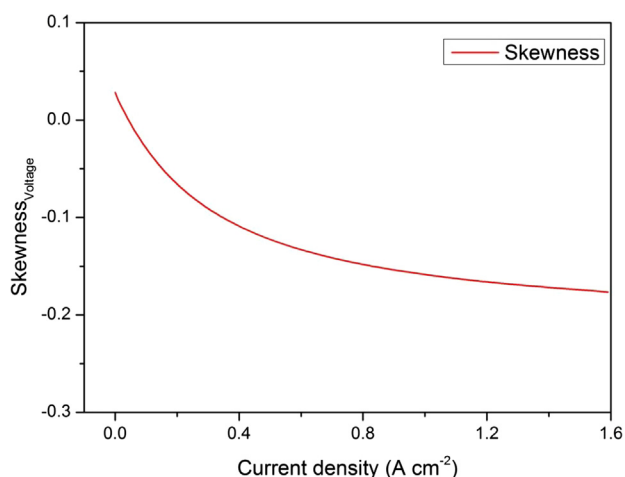
Fig. 6 – Skewness of V–I polarisation 'area' at operating temperature of 80 °C and standard deviation of ±5 °C.

configuration shown in Fig. 2). The fans are powered by a programmable power supply (3649A Agilent), and the fuel cell was loaded using an Agilent 6060B load unit; each controlled using bespoke software (LabVIEW, National Instruments) using a GPIB interface. Each of the 5 cells has a membrane surface area of 60 cm².

Due to its unique design, it does not require any external heating and operates from room temperature. Heat is generated by the electrochemical reactions and Joule heating.

A K-type thermocouple was used to record the internal temperature in the central area of the fuel cell and operate the PID controller. The PID controller treats the temperature as an input, and changes the speed of the fans in order to regulate the temperature to its predefined setpoint.

3.2. Heat management and thermal imaging

Temperature mapping, either with thermocouples [43–46], micro sensors measuring the temperature and humidity [47], thermistors [48], thermal imaging [23] [49–54], of fuel cells has shown to be a powerful tool to understand the performance and validate heat transfer models. The open-cathode configuration of the AC stack makes it an ideal system for thermal imaging because it is possible to directly point the camera at the active and cooling channels.

Thermal imaging was performed using a 640 × 512 focal plane array InSb camera (SC5600MB FLIR, UK). The camera was calibrated for the temperature range in question (15–100 °C) with the images being recorded using commercially available software (ResearchIR, FLIR ATC, Croissy-Beaubourg, France). Images were recorded at a frequency of 25 Hz for a period greater than 10 min to ensure a statistically significant number of data points were collected.

4. Results and discussion

4.1. Analytical interpretation

The analytical approach provides insight into the physics of the system and how temperature makes an impact on

performance. Fig. 3 shows the variation in differential cell voltage with respect to temperature as a function of current density and absolute operating temperature. It can be seen that the PEFC becomes more sensitive to temperature change with increasing current density and reduced temperature; increasing to over 10 mV °C^{-1} above 1 A cm^{-2} from 30 to 90 °C.

The effect of temperature on the various loss mechanisms can be seen in Fig. 4. The following observations can be made: (i) the entropy change associated with the formation of water leads to a small change in OCV over this temperature range; (ii) electro-kinetics improve with temperature resulting in lower activation loss due to exponential increase in ORR i_0 with temperature; (iii) Ohmic loss increases linearly with current, increased temperature results in a reduction of the resistance inside the cell due to increased proton conductivity; (iv) concentration loss, which is mainly dominant at higher
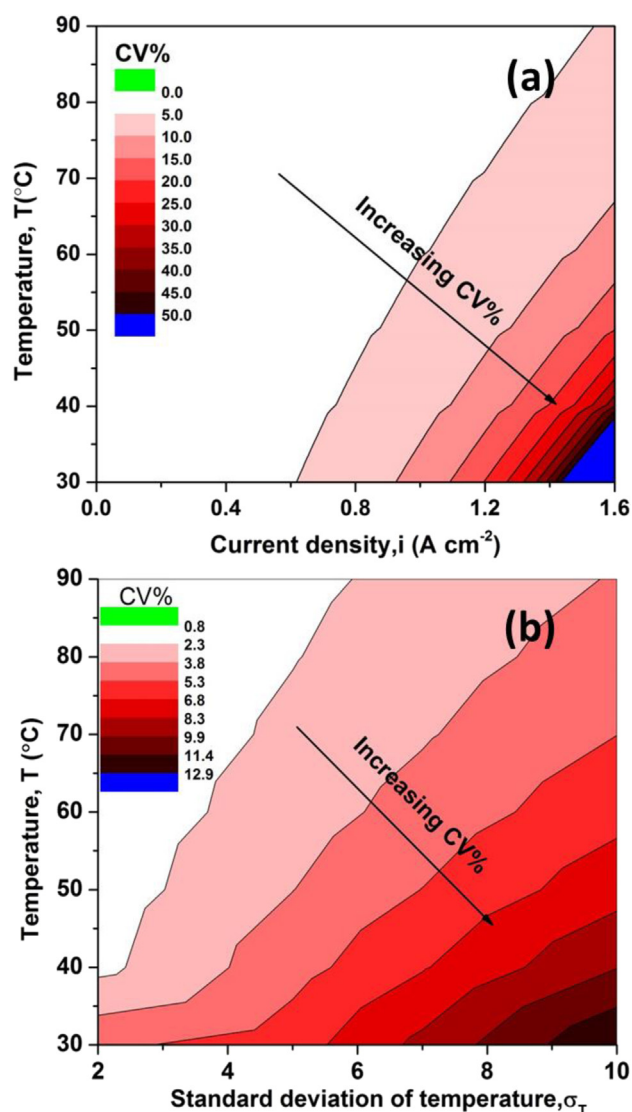

Fig. 7 – Contour plots showing: (a) how CV changes at different mean operating temperatures for ±5 °C; (b) how CV changes at an operating temperature of 80 °C with various standard deviation of temperature uncertainty at i = 0.6 A cm^{-2}.
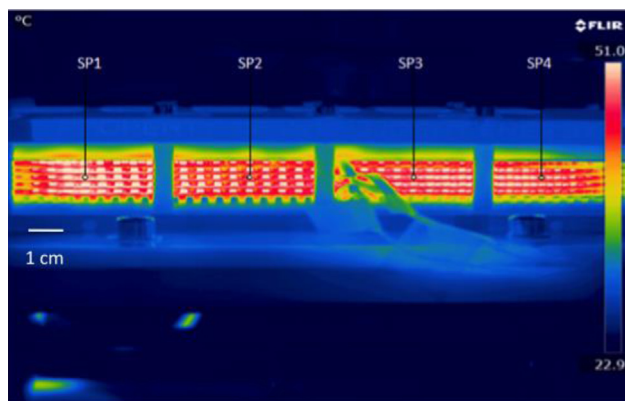
Fig. 8 – Thermal image of fuel cell stack at a current loading of 46 A (0.78 A cm^{-2}) after equilibrating for 25 min.

current density, also reduces with temperature due to improved diffusion, gas mobility and species concentration resulting in better mass transport and larger limiting current density.

4.2. Statistical interpretation

To capture the probabilistic behaviour of cell performance under temperature uncertainly, MCS sampling was used to provide temperature input samples for a mean operating temperature of 80 °C and standard deviation of ±5 °C. The samples generated by MCS are introduced into the deterministic lumped mathematical PEFC model to obtain cell voltage for various current densities.

It is apparent from Fig. 5 that voltage distribution is not uniform at different current densities. The colour map shows that as current density increases, the width of the distribution increases. This figure clearly shows that the expectation of a polarisation response to conform to a single 'line' is not reasonable when there is uncertainty associated with temperature (or other operating parameters). Rather, a polarisation 'area' or 'band' better describes the situation.

It can be seen in Fig. 5 that performance shows higher sensitivity at larger current density due to non-linearity of the model which is more dominant at higher current density.

To calculate the degree of asymmetry of a distribution over various current densities, the skewness is determined to show the effect of temperature variation on cell performance. It can be seen in Fig. 6, there is a tendency towards lower voltage in the $V–I$ polarisation area due to higher overpotential and probabilistic effect of temperature on the cell performance. It can be seen that skewness of the voltage distribution becomes more negative with increased current density, i.e. fuel cell voltage will be more likely to be biased towards lower voltage. To establish the extent of skewness, Equation (5) is used to determine the SES. The results show that over a current density of 0.2 A cm^{-2} the magnitude of the skewness is larger than twice the SES. This indicates that the distribution can be regarded as significantly skewed towards a lower voltage with increasing current.

Fig. 7(a) shows how CV changes at different operating temperatures (30–90 °C), taking a temperature uncertainty of ±5 °C. The trend across current and temperature is qualitatively the same as that observed in the analytical analysis; however, this interpretation allows the probability at each condition to be quantified.
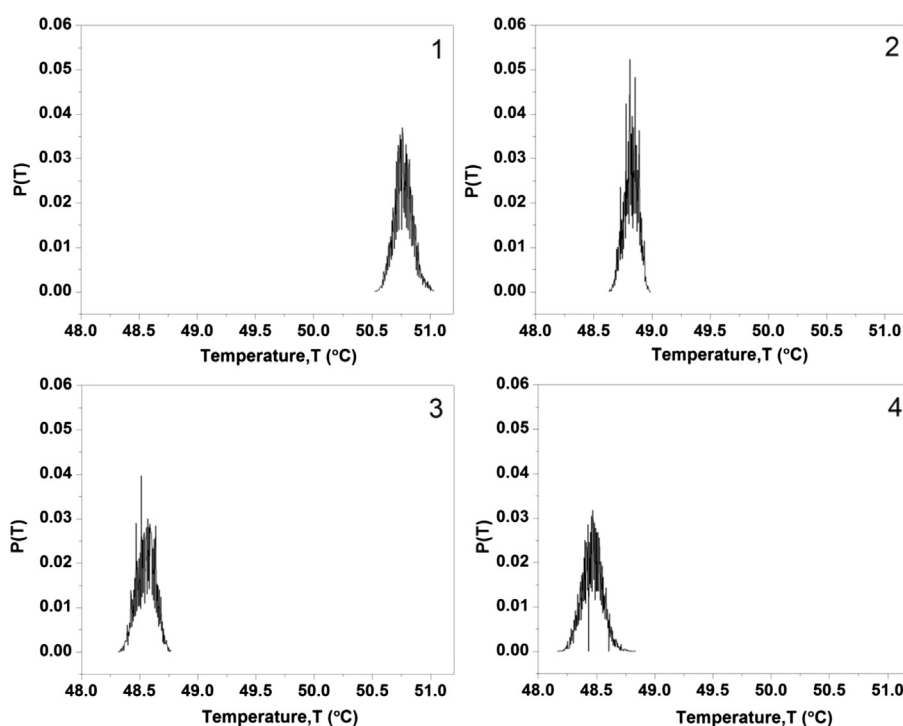

Fig. 9 – Temperature distribution after 25 min fuel cell operation at current density 0.78 A cm^{-2}. Figs. 1–4 show the four points (SP1–SP4) along the middle cell. SP1 is the closest point to H$_2$ entrance and SP4 is the furthest.

Table 4 – -Statistical variables for four points along the MEA at current density 0.78 A cm^{-2} after 25 min of data collection.

Statistical variables	SP1	SP2	SP3	SP4
Mean	50.8	48.8	48.5	48.5
CV%	0.044	0.041	0.037	0.08
Skewness	1.4×10^{-13}	1.3×10^{-13}	8.6×10^{-14}	5.2×10^{-14}

To establish how dispersion of cell voltage relates to the given temperature uncertainty, the CV of cell voltage is calculated for different σ_T values at a current density of 0.6 A cm^{-2} (Fig. 7(b)). It can be seen that regardless of temperature uncertainty the σ_T increases monotonically.

4.3. Stack testing

4.3.1. Thermal imaging
Thermal imaging measurements achieved a pixel resolution of ~0.35 mm. The noise-equivalent temperature difference (NETD), a measure of the signal-to-noise ratio, of the camera during the experiments was recorded as 19 mK, demonstrating a high thermal resolution.

A calibration was conducted in order to eliminate environmental reflections. To achieve this, a diffuse reflector was used to enable the environmental emissivity to be set to unity. In investigating the temperature distribution of the stack, each channel represented a cavity that could be considered to be a quasi-black body [55]. This allows an emissivity approaching unity to be used; in this case, 0.98 was chosen. By utilising this technique a direct comparison can be made between the active and cooling channels without the need to calculate the emissivity of each channel.

Fig. 8 shows a thermal image of the stack seen from the side with air exiting the system. It can be seen that there is substantial temperature variation across the stack with ~12 °C difference between the active and cooling channels (active —white and cooling — red). The figure also shows the position of four different point measurements (SP1–SP4) made along the central cell in the stack, used to assess lateral temperature variation in space and time.

4.3.2. Statistical interpretation of experimental temperature distribution
The temporal temperature distribution for each of the four points displays a Gaussian distribution (Fig. 9), the statistical characterisation for each point is shown in Table 4. It can be seen that the CV of location 1 to location 4 increases by almost 50% showing that the spatial distribution itself has ranging temporal variation. Also in the same table it can be seen that the skewness is effectively zero.

5. Conclusion

Temperature is a key parameter for determining PEFC performance and uncertainty in this parameter is reflected in the variability in the polarisation response. An analytical and statistical approach has been used to determine the sensitivity and probability of performance variation as a function of current density and nominal operating temperature.

Lower cell temperatures and higher current densities are predicted to lead to the greatest variation in performance for a given temperature change or statistical variation ('uncertainty'). The study has identified an effective polarization 'area' or 'band', in contrast to the widely quoted polarization 'curve', as being the most appropriate way to represent model predictions of fuel cell performance.

The cell performance variation due to temperature distribution at a given point in the V–I polarisation area translates into the negative skewness. This means that there is a tendency for the V–I area to be biased towards a lower voltage. Therefore, reported polarisation data will tend to err on the side of poorer perceived performance due to the natural variation in temperature for a given system.

Thermal imaging on an operational PEFC stack allows the spatial and temporal variation in temperature to be assessed. The experiments show that the width of temperature distribution decreases spatially towards the "dead-end" of the stack. A temperature variation of over 12 °C was observed across the active area of the stack (air exit face), whereas the variation across the central MEA was ~2.5 °C and the temporal variation has a standard deviation of ±0.5 °C.

REFERENCES

[1] Springer TE, Zawodzinski TA, Gottesfeld S. Polymer electrolyte fuel cell model. J Electrochem Soc 1993;138(8):2334–42.

[2] Sammes N, Boersma R. Small-scale fuel cells for residential applications. J Power Sources Mar. 2000;86(1–2):98–110.

[3] Zhang Z, Huang X, Jiang J, Wu B. An improved dynamic model considering effects of temperature and equivalent internal resistance for PEM fuel cell power modules. J Power Sources Oct. 2006;161(2):1062–8.

[4] Yalcinoz T, Alam M. Improved dynamic performance of hybrid PEM fuel cells and ultracapacitors for portable applications. Int J Hydrogen Energy Apr. 2008;33(7):1932–40.

[5] El-Sharkh MY, Rahman A, Alam MS, Byrne PC, Sakla AA, Thomas T. A dynamic model for a stand-alone PEM fuel cell power plant for residential applications. J Power Sources Nov. 2004;138(1–2):199–204.

[6] El-Sharkh MY, Rahman A, Alam MS. Neural networks-based control of active and reactive power of a stand-alone PEM

fuel cell power plant. J Power Sources Sep. 2004;135(1–2):88–94.

[7] Mert SO, Dincer I, Ozcelik Z. Exergoeconomic analysis of a vehicular PEM fuel cell system. J Power Sources Feb. 2007;165(1):244–52.

[8] Gencoglu MT, Ural Z. Design of a PEM fuel cell system for residential application. Int J Hydrogen Energy Jun. 2009;34(12):5242–8.

[9] Yilanci A, Dincer I, Ozturk H. Performance analysis of a PEM fuel cell unit in a solar–hydrogen system. Int J Hydrogen Energy Dec. 2008;33(24):7538–52.

[10] Nguyen TV, White RE. A water and heat management model for proton-exchange-membrane fuel cells. J Electrochem Soc 1993;140(8).

[11] Ang SMC, Brett DJL, Fraga ES. A multi-objective optimisation model for a general polymer electrolyte membrane fuel cell system. J Power Sources 2010;195:2754–63.

[12] Das PK, Li X, Liu Z-S. Analysis of liquid water transport in cathode catalyst layer of PEM fuel cells. Int J Hydrogen Energy Mar. 2010;35(6):2403–16.

[13] Das PK, Li X, Xie Z, Liu ZS. Effects of catalyst layer structure and wettability on liquid water transport in polymer electrolyte membrane fuel cell 2011;(June):1325–39.

[14] Mawardi A, Pitchumani R. Effects of parameter uncertainty on the performance variability of proton exchange membrane (PEM) fuel cells. J Power Sources 2006;160:232–45.

[15] Srinivasulu GN, Subrahmanyam T, Rao VD. Parametric sensitivity analysis of PEM fuel cell electrochemical Model. Int J Hydrogen Energy 2011;36(22):14838–44.

[16] Tao WQ, Min CH, Liu XL, He YL, Yin BH, Jiang W. Parameter sensitivity examination and discussion of PEM fuel cell simulation model validation part I. Current status of modeling research and model development. J Power Sources 2006;160:359–73.

[17] Min CH, He YL, Liu XL, Yin BH, Jiang W, Tao WQ. Parameter sensitivity examination and discussion of PEM fuel cell simulation model validation part II: results of sensitivity analysis and validation of the model. J Power Sources 2006;160:374–85.

[18] Yan W-M, Chen C-Y, Mei S-C, Soong C-Y, Chen F. Effects of operating conditions on cell performance of PEM fuel cells with conventional or interdigitated flow field. J Power Sources Nov. 2006;162(2):1157–64.

[19] Correa G, Borello F, Santarelli M. Sensitivity analysis of temperature uncertainty in an aircraft PEM fuel cell. Int J Hydrogen Energy Nov. 2011;36(22):14745–58.

[20] Pharoah JG, Burheim OS. On the temperature distribution in polymer electrolyte fuel cells. J Power Sources 2010;195(16):5235–45.

[21] Shimpalee S, Dutta S. Distribution in PEM fuel cells. Numer Heat Trans 2000;38:111–28.

[22] Aieta NV, Das PK, Perdue A, Bender G, Herring AM, Weber AZ, et al. Applying infrared thermography as a quality-control tool for the rapid detection of polymer-electrolyte-membrane-fuel-cell catalyst-layer-thickness variations. J Power Sources Aug. 2012;211:4–11.

[23] Hakenjos A, Muenter H, Wittstadt U, Hebling C. A PEM fuel cell for combined measurement of current and temperature distribution, and flow field flooding. J Power Sources 2004;131:213–6.

[24] Daino MM, Lu Z, LaManna JM, Owejan JP, Trabold TA, Kandlikar SG. Through-plane water transport visualization in a PEMFC by visible and infrared imaging. Electrochem Solid State Lett 2011;14(6):B51.

[25] Placca L, Kouta R. Effects of temperature uncertainty on the performance of a degrading PEM fuel cell model. J Power Sources 2009;194:313–27.

[26] Nguyen TV. An along-the-channel model for proton exchange membrane fuel cells. J Electrochem Soc 1998;145(4):1149–59.

[27] O'Hayre R, Cha S-W, Colella W, Prinz FB. Fuel cell fundamentals. 2nd ed. Wiley; 2009. pp. 25–194.

[28] Spiegel C. PEM fuel cell modeling and simulation using matlab. Academic Press; 2011. p. 456.

[29] Cussler EL. Diffusion mass transfer in fluid systems. Cambridge University Press; 2009. pp. 117–60.

[30] Bernardi DM, Verbrugge MW. A mathematical model of the solid-polymer-electrolyte fuel cell 1992;139(9).

[31] Nam JH, Kaviany M. Effective diffusivity and water-saturation distribution in single- and two-layer PEMFC diffusion medium. Int J Heat Mass Trans Nov. 2003;46(24):4595–611.

[32] Meng H, Wang C-Y. Electron transport in PEFCs. J Electrochem Soc 2004;151(3):A358.

[33] Das PK, Li X, Liu Z-S. Effective transport coefficients in PEM fuel cell catalyst and gas diffusion layers: beyond Bruggeman approximation. Appl Energy Sep. 2010;87(9):2785–96.

[34] Das PK, Li X, Liu Z-S. Analytical approach to polymer electrolyte membrane fuel cell performance and optimization. J Electroanal Chem Jun. 2007;604(2):72–90.

[35] Montgomery GC, Runger Douglas C. Continuous random variables and probability distributions. In: Applied statistics and probability for engineers, 3rd ed.: John Wiley & Sons, Inc. p. 97–140.

[36] Randn, MathWorks [Online]. Available: http://www.mathworks.co.uk/help/matlab/ref/randn.html.

[37] Eaton W. GNU octave manuals [Online]. Available: http://www.gnu.org/software/octave/doc/interpreter/; 1997.

[38] Weisstein EW, Skewness, MathWorld-A Wolfram web Resource [Online]. Available: http://mathworld.wolfram.com/Skewness.html.

[39] Bell M. Skew and how skewness is calculated in statistical software, Math/Chaos Theory Suite101 [Online]. Available: http://suite101.com/article/skew-and-how-skewness-is-calculated-in-statistical-software-a231005; 2009.

[40] Fleming Michael C, Nellis Joseph G. Describing data-variability. In: Nellis Joseph G, editor. Principles of applied statistics. 1st ed. New York: Routledge; 1994. pp. 54–7.

[41] Wu J, Galli S, Lagana I, Pozio A, Monteleone G, Yuan XZ, et al. An air-cooled proton exchange membrane fuel cell with combined oxidant and coolant flow. J Power Sources Mar. 2009;188(1):199–204.

[42] Santa Rosa DT, Pinto DG, Silva VS, Silva RA, Rangel CM. High performance PEMFC stack with open-cathode at ambient pressure and temperature conditions. Int J Hydrogen Energy Dec. 2007;32(17):4350–7.

[43] Wilkinson M, Blanco M, Gu E, Martin JJ, Wilkinson DP, Zhang JJ, et al. In situ experimental technique for measurement of temperature and current distribution in proton exchange membrane fuel cells. Fuel Cell 2006:507–11.

[44] Matian M, Marquis A, Brett D, Brandon N. An experimentally validated heat transfer model for thermal management design in polymer electrolyte membrane fuel cells. Proc Inst Mech Eng Part A J Power Energy Dec. 2010;224(8):1069–81.

[45] Zhang G, Guo L, Ma L, Liu H. Simultaneous measurement of current and temperature distributions in a proton exchange membrane fuel cell. J Power Sources 2010;195(11):3597–604.

[46] Lottin O, Colinart T, Chupin S, Didierjean S. A multi-instrumented polymer exchange membrane fuel cell: observation of the in-plane non-homogeneities. J Power Sources 2008;180:748–54.

[47] Lee C, Hsieh W, Wu G. Embedded flexible micro-sensors in MEA for measuring temperature and humidity in a micro-fuel cell. Fuel Cell 2008;181:237–43.

[48] He S, Mench MM, Tadigadapa S. Thin film temperature sensor for real-time measurement of electrolyte temperature in a polymer electrolyte fuel cell. Sensors Actuat 2006;125:170—7.

[49] Wang M, Guo H, Ma C. Temperature distribution on the MEA surface of a PEMFC with serpentine channel flow bed. J Power Sources 2006;157:181—7.

[50] Guo H, Hai M, Ye F, Fang C. Experimental study of temperature distribution on anodic surface of MEA inside a PEMFC with parallel channels flow bed. Int J Hydrogen Energy 2012;37(17):13155—60.

[51] Martins LS, Gardolinski JEFC, Vargas JVC, Ordonez JC, Amico SC, Forte MMC. The experimental validation of a simplified PEMFC simulation model for design and optimization purposes. Appl Thermal Eng 2009;29(14—15):3036—48.

[52] Shimoi R, Masuda M, Fushinobu K, Kozawa Y, Okazaki K. Visualization of the membrane temperature field of a polymer electrolyte fuel cell. J Energy Resour Technol 2004;126(December):258—61.

[53] Matian M, Marquis AJ, Brandon NP. Application of thermal imaging to validate a heat transfer model for polymer electrolyte fuel cells. Int J Hydrogen Energy Nov. 2010;35(22):12308—16.

[54] Brett DJL, Aguiar P, Clague R, Marquis AJ, Schöttl S, Simpson R, et al. Application of infrared thermal imaging to the study of pellet solid oxide fuel cells. J Power Sources Mar. 2007;166(1):112—9.

[55] Vollmer M, Mollmann K-P. Infrared thermal imaging-fundamentals, research and applications; 2010. Weinheim.